HHS Public Access

Author manuscript

Atherosclerosis. Author manuscript; available in PMC 2017 August 01.

Published in final edited form as:

Atherosclerosis. 2016 August ; 251: 226–233. doi:10.1016/j.atherosclerosis.2016.06.046.

Enhanced neointimal fibroblast, myofibroblast content and altered extracellular matrix composition: Implications in the progression of human peripheral artery restenosis

Prakash Krishnan[1], **K-Raman Purushothaman**[*,1], **Meerarani Purushothaman**, **Irene C. Turnbull**, **Arthur Tarricone**, **Miguel Vasquez**, **Sachin Jain**, **Usman Baber**, **Rheoneil A. Lascano**, **Annapoorna S. Kini**, **Samin K. Sharma**, and **Pedro R. Moreno**

The Zena and Michael A. Weiner Cardiovascular Institute, The Marie-Josée and Henry R. Kravis Cardiovascular Health Center, Department of Medicine/Cardiology, Icahn School of Medicine at Mount Sinai, New York, NY, USA

Abstract

Background and aims—Neointimal cellular proliferation of fibroblasts and myofibroblasts is documented in coronary artery restenosis, however, their role in peripheral arterial disease (PAD) restenosis remains unclear. Our aim was to investigate the role of fibroblasts, myofibroblasts, and collagens in restenotic PAD.

Methods—Nineteen PAD restenotic plaques were compared with 13 *de novo* plaques. Stellate cells (H&E), fibroblasts (FSP-1), myofibroblasts (α-actin/vimentin/FSP-1), cellular proliferation (Ki-67), and apoptosis (caspase-3 with poly ADP-ribose polymerase) were evaluated by immunofluorescence. Collagens were evaluated by picro-sirius red stain with polarization microscopy. Smooth muscle myosin heavy chain (SMMHC), IL-6 and TGF-β cytokines were analyzed by immunohistochemistry.

Results—Restenotic plaques demonstrated increased stellate cells (2.7 ± 0.15 *vs.* 1.3 ± 0.15) fibroblasts (2282.2 ± 85.9 *vs.* 906.4 ± 134.5) and myofibroblasts (18.5 ± 1.2 *vs.* 10.6 ± 1.0) $p = 0.0001$ for all comparisons. In addition, fibroblast proliferation (18.4% ± 1.2 *vs.* 10.4% ± 1.1; $p = 0.04$) and apoptosis (14.6% ± 1.3 *vs.* 11.2% ± 0.6; $p = 0.03$) were increased in restenotic plaques. Finally, SMMHC (2.6 ± 0.12 *vs.* 1.4 ± 0.15; $p = 0.0001$), type III collagen density (0.33 ± 0.06 *vs.* 0.17 ± 0.07; $p = 0.0001$), IL-6 (2.08 ± 1.7 *vs.* 1.03 ± 2.0; $p = 0.01$), and TGF-β (1.80 ± 0.27 *vs.* 1.11 ± 0.18; $p = 0.05$) were increased in restenotic plaques.

[*]Corresponding author. Icahn School of Medicine at Mount Sinai, Cardiovascular Institute, One Gustave Levy Place, New York, NY 10029, USA. purushothaman.kothandaraman@mountsinai.org (K.-R. Purushothaman).

[1]These authors contributed equally to this study.

Conflict of interest

The authors declared that they do not have anything to disclose regarding conflict of interest with respect to this manuscript.

Author contributions

Prakash Krishnan: planned and executed the study, reviewed and edited the manuscript; K-Raman Purushothaman and Meerarani Purushothaman: conducted scientific experiments, researched data, wrote, reviewed and edited the manuscript; Irene Turnbull worked in revised experiments and edited the revision; Usman Baber: analyzed the researched data; Arthur Tarricone, Miguel Vasquez, Rheoneil A. Lascano and Sachin Jain helped in research data and specimen collections; Annapoorna Kini, Samin Sharma and Pedro Moreno supervised the planning and execution of the clinical study, reviewed and edited the manuscript.

Conclusions—Our study suggests proliferation and apoptosis of fibroblast and myofibroblast with associated increase in type III collagen may play a role in restenotic plaque progression. Understanding pathways involved in proliferation and apoptosis in neointimal cells, may contribute to future therapeutic interventions for the prevention of restenosis in PAD.

Keywords

Atherosclerosis; Neointimal proliferation; Peripheral arterial disease; Restenosis; Collagens

1. Introduction

Symptomatic peripheral arterial disease (PAD) restenosis remains a frequent complication of percutaneous intervention, increasing cardiovascular morbidity and mortality [1–5]. The specific mechanisms and histopathological findings leading to PAD restenosis involve inflammatory cell activation, cytokine production, smooth muscle cell (SMC) proliferation, apoptosis and collagen production [6]. Inflammatory cells like macrophages are well studied in coronary and peripheral arterial restenosis [7–9]. However, additional vascular cells may play a role in this proliferative process. Conventionally, resident intimal SMC proliferation plays a major role in restenosis [10]. SMCs include thin (α-actin positive) and thick (smooth muscle myosin heavy chain- SMMHC) filaments [11]. Other non-resident cells like fibroblast and myofibroblast, derived from the interstitial connective tissue beneath the subintimal layer of the atherosclerotic plaque, may contribute to the restenotic process. Fibroblasts and myofibroblasts may migrate into the neointima mediated by cytokines [12]. These cells along with the resident SMCs may proliferate and eventually undergo apoptosis mediated by caspase-3, and also contribute collagen deposition and neointimal expansion. Although caspase-3 plays a key role as effector in apoptosis, it also facilitates other cellular events in cell differentiation and development [13]. Furthermore, downstream effect of apoptosis is played by Poly (ADP-ribose) polymerase (PARP), DNA-binding enzyme which detects and signals DNA strand breaks [14]. PARP is activated at an intermediate stage of apoptosis and is then cleaved and inactivated at a late stage by caspase-3 and other proteases [14]. The biological presence of PARP indicates the cleaved end products of apoptosis mediated by caspase-3. In addition, interstitial fibroblasts and myofibroblasts synthesize the cytokines IL-6 and TGF-β [15]. IL-6 is involved in the migration of fibroblasts, and mediates signal transdifferentiation into myofibroblast [16,17]. In addition, TGF-β may contribute to transdifferentiation of the fibroblast intomyofibroblast by inducing activation of α-smooth muscle actin (α-SMA) [18]. These epithelial mesenchymal transdifferentiation (EMT) from fibroblast to myofibroblast may contribute to extracellular matrix collagen synthesis [19–22]. Furthermore, resident neointimal SMCs and stellate cells will enhance neointimal collagen content. Therefore, neointimal fibroblast and myofibroblast may be crucial in type III collagen synthesis, leading to neointimal expansion [23,24]. These cells were extensively studied previously in coronary artery restenosis [25–29]. However, the role of fibroblast and myofibroblast in PAD restenosis has not been well studied. This study sought to investigate a possible association of increased fibroblast and myofibroblast composition with type III collagen deposition in restenotic plaques from patients with PAD.

2. Materials and methods

2.1. Tissue collection

A total of thirty-two plaque specimens were collected from twenty-four patients during atherectomy procedures using the SilverHawk atherectomy device (Fox Hollow Technologies, Redwood City, CA) at the cardiac catheterization laboratory, Mount Sinai Hospital. Nineteen restenotic plaque specimens were procured from 12 patients (8 female and 4 male) and thirteen control *de novo* plaques were procured from 12 patients (2 female and 10 male). All plaque samples were collected from superficial femoral arterial branch, and within 20 min, washed in saline and fixed in 10% buffered formalin and immediately submitted for processing into paraffin blocks. This study was approved by the institutional review board at the Icahn School of Medicine at Mount Sinai, New York. All the specimen procurements were done after informed consent was obtained for experimentation in human subjects. Also, this study conforms to the Declaration of Helsinki. Relevant demographic and clinical profiles were collected from case records and analyzed.

2.2. Quantification of stellate cell grade

Stellate cells were quantified using hematoxylin & eosin staining by evaluating cells resembling “stellate” shape appearance admixed in the loose myxoid and clear background (representing active myofibroblast) and histologically graded for the presence of stellate shaped cells per high-power field (HPF) as follows; Grade-1: scant to minimal stellate cells (occupying ≤ 25% of HPF), Grade-2: moderate stellate cells (occupying > 25%–75% of HPF), and Grade-3: dense stellate cells (occupying > 75% of HPF), in the neointima. A total of 10 randomly selected HPFs were used for the analysis.

2.3. Quantification of fibroblast content

Immunohistochemistry was performed using specific primary antibodies, rabbit polyclonal FSP-1 (ab27957, Abcam Inc., MA, 1:100 dilution) as a pan fibroblast marker. Appropriate secondary antibodies and positive (human skin) and negative (rabbit IgG from Dako, CA) controls were included to distinguish non-specific binding. Using FSP-1 immunostained sections, the total number of positively stained FSP-1 in ten random HPF (20×) for each plaque were enumerated. The total plaque area occupied in a HPF was measured in mm^2 using a computerized planimetry system. The density of FSP-1 positive stained cells was calculated by dividing the total number of FSP-1 positive stained cells by the total plaque area measured per HPF.

2.4. Quantification of smooth muscle cell myosin heavy chain (SMMHC) content

Immunochemistry was performed using specific, non-cross reacting rabbit polyclonal antibody against SMMHC (ab124679, Abcam, MA, 1:100 dilution). Appropriate positive controls for SMMHC (human colon) and negative controls (rabbit IgG from DAKO, CA) were included. Sections were examined under an Olympus BX 50 light microscope (Olympus America, Center Valley, PA), and the expression of SMMHC was quantified in 20 random high-power fields (HPFs) using percentage of positive cells stained per HPF. Using the intensity of cells immunostained with SMMHC, a semi quantitative score was used to

grade as follows; grade 0: absent, grade 1: 25% stained, grade 2: 26%–50% stained, grade 3: >50 stained.

2.5. Quantification of myofibroblast content

Myofibroblasts are histologically defined as α-SMA positive cells, co-expressing fibroblast and vimentin markers. Myofibroblast cellular content was quantified using the percentage of cells expressing all these three markers. To detect myofibroblasts, immunofluorescent labeling with combined primary antibodies against the following antigens were adopted, rabbit polyclonal FSP-1 (ab27957-Abcam, MA, 1:100 dilution), mouse monoclonal α-SMA (α-SMA-FITC, F3777-Sigma Aldrich, MO, 1:500 dilution), and vimentin (ab45939-Abcam, MA, 1:100 dilution). Secondary antibodies, donkey anti-mouse Alexa Fluor 488 or anti-rabbit Alexa Fluor 594 (A-21202 and A-21207, respectively; Invitrogen, NY, 1:500 dilution) were used. Mounting medium containing DAPI (H-1200-Vector Lab, CA) was then applied. Quantification of the co-expression of α-SMA with FSP-1, and α-SMA with vimentin (myofibroblast) were performed in a blinded fashion. Cellular co-expression of randomly selected images captured at 20× magnification were quantified. Combined cellular co-expression of α-SMA with FSP-1 and α-SMA with vimentin (myofibroblast) were analyzed and scored as percentage of positive myofibroblast cell content. Images were acquired using the Leica TCS SP5 DMI, inverted confocal laser scanning microscope at Mount Sinai's Shared Resource Facility and analyzed using Leica LAS AF lite software system.

2.6. Quantification of cellular proliferation and apoptosis

Subgroup analysis from the same group of plaques in restenosis and *de novo* was performed for the intimal resident cells that proliferate and undergo apoptosis by quantifying the number of FSP-1 and α-SMA expressing cells that co-express Ki67 and caspase-3 by immunofluorescence staining and confocal microscopy. Primary antibodies against the following antigens were used: rabbit polyclonal FSP-1 (ab27957-Abcam, MA), mouse monoclonal α-SMA (FITC-F3777-Sigma Aldrich, MO, 1:500 dilution), rabbit monoclonal Ki-67 (ab16667-Abcam, MA, 1:100 dilution), and caspase-3 (ab44976-Abcam, MA, 1:200 dilution). Additionally, controls were included in parallel by substituting the primary antibody for IgG or specific IgG isotypes from the same species and at the same final concentration as the primary antibody. Secondary antibodies donkey anti-mouse Alexa Fluor 488 or anti-rabbit Alexa Fluor 594 (A-21202 and A-21207, respectively; Invitrogen, NY, 1:500 dilution) were used. Mounting medium containing DAPI (H-1200-Vector Lab, CA) was then applied. Quantification of FSP-1 expressing Ki-67 and caspase-3 was performed in a blinded fashion. Cellular co-localization in randomly selected images captured at 20× magnification was quantified. Images were acquired using Leica TCS SP5 DMI, inverted confocal laser scanning microscope at Mount Sinai's Shared Resource Facility and analyzed using Leica LAS AF lite software system.

In addition, the cleaved end product of (caspase-3 mediated) apoptotic process, PARP was detected as a surrogate marker that was identified in caspase-3 positive cells. Primary antibodies against the rabbit polyclonal caspase-3 (ab44976-Abcam, MA, 1:200 dilution), and mouse monoclonal anti-PARP antibody (ab110915-Abcam, MA, 1:100 dilution) were used. Controls were included in parallel as mentioned above. Secondary antibodies anti-

rabbit Alexa Fluor 594 or donkey anti-mouse Alexa Fluor 488 (A-21207 and A-21202, respectively; Invitrogen, NY, 1:500 dilution) were used. Immunofluorescence evaluations were done using EVOS FL microscope (Thermo Fisher Scientific, MA). Analysis of the percentage of signal co-expression was done using Image J-software (NIH).

2.7. Quantification of collagen density

Plaque tissue sections were stained with picro-sirius red and used to quantify type I collagen and type III collagen as published previously [30]. The total plaque area was measured at 20× magnification by light microscopy. The same plaque area was then polarized and the color intensities for type I collagen in the red polarized area and type III collagen in the green/yellow polarized area were measured by planimetry using manual tracing of the color intensities and calibrated using Zedec-QuantIm software attached with a pre-calibrated scale. The area occupied by individual type I and III collagen was quantified in the entire intimal plaque area and divided by the total intimal plaque area in HPF and expressed as collagen density per mm^2.

2.8. Quantification of IL-6 and TGF-β

Immunohistochemistry was performed using specific, non-cross reacting rabbit polyclonal antibody against IL-6 (ab6672, Abcam, MA, 1:200 dilution) and mouse monoclonal antibody against TGF-β (ab27969, Abcam, MA, 1:200 dilution). Appropriate positive controls were used for IL-6 (human tonsil), and TGF-β (human liver) and negative controls (rabbit and mouse IgG from DAKO, CA) were included. Sections were examined under an Olympus BX 50 light microscope (Olympus America, Center Valley, PA), and the expression of IL-6 and TGF-β were quantified in 20 random high-power fields (HPFs) using percentage of positive cells stained per HPF. Using a modified protocol of a previously published methodology [13], a semi quantitative score was used to grade as follows: grade 0: absent; grade 1: 1%–25%; grade 2: 26%–50%; grade 3: 50–100%.

2.9. Statistical analysis

Data are presented as mean ± SEM. For 2-group comparisons, Gaussian-distribution samples were juxtaposed with the 2-tailed Student's t-test and were preceded by a Levene F test for equality of variances. Non-Gaussian-distribution samples were compared by the Mann-Whitney nonparametric test. IBM SPSS/PASW 20.0 software (SPSS Inc., Chicago, IL) was used for the analysis. A value of $p = 0.05$ was considered statistically significant.

3. Results

Patient age was similar in both groups ($p = 0.80$). There were fewer males in restenotic group compared to the *de novo* group ($p = 0.02$). With the exception of gender, body mass index and rest pain in lower limbs, all other clinical parameters showed no significant difference between the groups (Table 1). Our study infers an interesting pattern of gender distribution, evidencing more female subjects in restenosis with 58% compared to 15% in *de novo* control group, and the majority of the women were postmenopausal. While it is most likely the interventional injury was the major trigger in inducing cellular and ECM changes

in restenosis, female gender may also represent a potential risk group in cellular fibrosis as observed recently [31].

3.1. Stellate cell, fibroblast, smooth muscle heavy chain and myofibroblast content

The mean stellate cell grade observed showed an increase in restenotic plaques compared to *de novo* plaques (2.7 ± 0.15 *vs.* 1.3 ± 0.15; $p = 0.0001$) (Fig. 1A–C). Fibroblast content was significantly increased in restenotic plaques compared to *de novo* plaques (2282.2 ± 85.9 *vs.* 906.4 ± 134.5; $p = 0.0001$) (Fig. 1D–F). The mean SMMHC grade observed was higher in restenotic plaques compared to *de novo* plaques (2.6 ± 0.12 *vs.* 1.4 ± 0.15; $p = 0.0001$) (Fig. 1G–I). The mean percentage of myofibroblast components evaluated using FSP-1 and α-SMA was increased in restenotic plaques compared to *de novo* plaques (18.5 ± 1.2 *vs.* 10.6 ± 1.0; $p = 0.0001$) (Fig. 2A–G). Similarly, the mean percentage of myofibroblast content, assessed by counting cells co-expressing α-SMA and vimentin, was increased in restenotic plaques compared to *de novo* plaques (23.3% ± 1.9 *vs.* 17.9% ± 1.5; $p = 0.04$) (Fig. 2H–N).

3.2. Percentage of fibroblast proliferation (FSP-1/Ki67)

The mean percentage of fibroblast proliferation evaluated by counting cells co-expressing FSP-1 and Ki-67 was significantly increased in restenotic plaques when compared to *de novo* plaques (18.4% ± 1.2 *vs.* 10.4% ± 1.1; $p = 0.0001$) (Fig. 3A–F).

3.3. Percentage of fibroblast apoptosis (FSP-1/Caspase-3)

The mean percentage of fibroblast apoptosis assessed by counting cells co-expressing FSP-1 and caspase-3 was increased in restenotic plaques compared to *de novo* plaques (14.6% ± 1.3 *vs.* 11.2% ± 0.6; $p = 0.03$) (Fig. 3G–L).

3.4. Percentage of smooth muscle cell proliferation (α-SMA/Ki-67)

The mean percentage of SMC proliferation as evaluated by co-expression of α-SMA and Ki-67 was significantly increased in restenotic plaques compared to *de novo* plaques (24.1% ± 2.1 *vs.* 17.52% ± 1.2; $p = 0.02$) (Fig. 3M–R).

3.5. Percentage of smooth muscle cell apoptosis (α-SMA/Caspase-3)

The mean percentage of SMC apoptosis assessed by counting cells that co-expressed α-SMA and caspase-3 was significantly increased in restenotic plaques when compared to *de novo* plaques (20.38% ± 1.8 *vs.* 10.08% ± 0.4; $p = 0.0001$) (Fig. 3S–X). Furthermore, the mean percentage of cells co-expressing caspase-3 and PARP was increased in restenotic plaques compared to *de novo* plaques (28.7 ± 0.9 *vs.* 11.8 ± 0.6; $p = 0.0001$) (Fig. 3A1–F1).

3.6. Collagen density

Type III collagen density was significantly increased in restenotic plaques compared to *de novo* plaques (0.33 ± 0.06 *vs.* 0.17 ± 0.07; $p = 0.0001$). In contrast, type I collagen density was significantly reduced in restenotic plaques compared to *de novo* plaques (0.14 ± 0.01 *vs.* 0.44 ± 0.02; $p = 0.0001$) (Fig. 4A–D).

3.7. Interleukin-6 and TGF-β grade

The presence of pro-inflammatory cytokine IL-6 and TGF-β, measured by using a scoring system assigning a grade as indicator of their abundance, resulted in a higher grade (2.08 ± 1.7 *vs.* 1.03 ± 2.0, $p = 0.01$ and 1.80 ± 0.27 *vs.* 1.11 ± 0.18; $p = 0.05$), in restenotic plaques compared to *de novo* plaques (Fig. 5A–F).

4. Discussion

In this study, we have characterized differences in the histopathological phenotype of restenotic versus *de novo* peripheral atherosclerotic plaques. In particular, an increased proliferation of stellate cells, fibroblasts and myofibroblasts were seen in restenotic plaques. In particular, we have noticed an enhanced proliferative and apoptotic activity of these cells in restenosis compared to *de novo* plaques.

The classical and traditional pattern of the restenotic process involves resident SMCs in the intima and the SMCs that transmigrated from the tunica media through the internal elastic lamellar disruption (IELD) [32]. These cells may proliferate, synthesize collagen and eventually undergo apoptosis under the regulation of macrophage-derived cytokines [33–35]. Similarly, fibroblast and myofibroblast derived from the subjacent tunica media/adventitia may also transmigrate through IELD into the neointima [36,37]. Nevertheless, they have not been well characterized histopathologically in human PAD restenosis. Fibroblasts are phenotypically resident interstitial cells characterized by the expression of Fibroblast Specific Protein-1 (FSP-1) [18]. The myofibroblasts can be immunohistologically distinguished by co-expression of FSP-1/α-SMA with vimentin [38,39]. Using the specific phenotype markers for fibroblast and myofibroblast, this study characterized the content of these cells, and evidenced an enhanced proliferative and apoptotic activity in restenotic plaques. In addition, IL6 may be associated with cell proliferation and apoptosis [40,41]. TGF-β has a complex role, its downstream effects involve both apoptosis and cell proliferation, and these end results are cell type-dependent [42]. Increase in TGF-β, α-SMA and collagen have been documented in fibrotic response [43]. When quantified in this study, cytokines IL6 and TGF-β were significantly increased in restenotic plaques.

To measure the apoptotic pathway of cells in neointima, the catalytic enzyme caspase-3 was used as marker. Furthermore, to specifically address the exact role of caspase-3 in apoptosis, downstream pathway end product PARP was measured. PARP is one of the essential substrates cleaved by caspase-3, an abundant DNA binding enzyme that detects and signals DNA strand breaks [14]. The presence of cleaved PARP is one of the most useful diagnostic tools for the detection of apoptosis in many cell types and indicative of caspase-3 activity [44]. In this study we have demonstrated an increase in PARP cleaved proteins in restenotic plaque compared to *de novo* plaque.

Finally, reparative type III collagen density was significantly increased, whereas mature type I collagen density was reduced in restenotic plaques. Previous studies documented collagen production by fibroblasts [19] suggesting a role for these cells in human PAD restenosis.

Migratory, non-resident mesenchymal cells like activated fibroblast and myofibroblast characterized neointima in coronary artery restenosis [25–28,45]. However, it is unclear if PAD restenosis also follows this pattern. Altered pathophysiological mechanisms and phenotypic population of cellular and matrix constituents needed to be studied to clarify this issue. Our present study provides observational evidence that suggests a role of fibroblast and myofibroblast in PAD restenosis. Apoptosis of smooth muscle cells and possibly fibroblasts was reported in a porcine model of coronary angioplasty; the type of cells and the rate at which they underwent proliferation or apoptosis varied across vascular wall regions and layers [46]. The role of fibroblasts in arterial restenosis has been evaluated in different animal models; the degree in which myofibroblasts are implicated in neointima formation in restenosis depends on the type of model and techniques used for cell identification among others, with the majority of studies supporting an active participation of fibroblasts after vascular injury, whereby they undergo differentiation and migration from the adventitia to the neointima [47]. Understanding cell differences in neointima PAD composition may contribute to future developments in therapeutic prevention of restenosis in PAD.

The number of patients in our study was limited. Since it is a retrospective study, fresh tissues for quantification of gene or protein expression was not available. Given the cross-sectional nature of our study design, we cannot infer a causal relationship between the histopathological phenotype observed in restenotic plaques and luminal narrowing. Since myofibroblasts represent a combination of cellular co-expression with α-SMA, fibroblast and vimentin, proliferative and apoptotic activity evaluation was not performed as a distinct myofibroblast single cell entity due to technical difficulty.

In conclusion, this study demonstrates increased stellate cell content, fibroblast, myofibroblast proliferation and apoptosis, with type III collagen production in human PAD restenosis. Furthermore, association of increased IL-6 and TGF-β cytokines may contribute to cellular events mediating apoptosis and proliferation that may contribute to neointima formation. In addition, fibroblast and myofibroblast involvement in neointimal proliferation leading to luminal narrowing may contribute to the severity of the restenotic lesion progression and clinical manifestations seen in symptomatic PAD. The underlying molecular mechanistic pathways that may be associated with cellular proliferation including apoptosis and type III collagen are under investigation.

Acknowledgments

Financial support

The authors acknowledge funding from Cardiovascular Institute and Endovascular Interventional Surgery, Icahn School of Medicine at Mount Sinai, New York and US National Institutes of Health (NIH)/NHLBI through grant T32-HL007824-18 (to I.C.T.).

Confocal microscopy was performed at the Shared Microscopy CORE at the Icahn School of Medicine at Mount Sinai.

References

1. Bouisset F, Bongard V, Ruidavets JB, et al. Prognostic usefulness of clinical and subclinical peripheral arterial disease in men with stable coronary heart disease. Am. J. Cardiol. 2012; 110:197–202. [PubMed: 22513182]
2. Welten GM, Schouten O, Chonchol M, et al. Prognosis of patients with peripheral arterial disease. J. Cardiovasc. Surg. (Torino). 2009; 50:109–121.
3. Criqui MH. Systemic atherosclerosis risk and the mandate for intervention in atherosclerotic peripheral arterial disease. Am. J. Cardiol. 2001; 88:43J–47J.
4. Criqui MH. Peripheral arterial disease–epidemiological aspects. Vasc. Med. 2001; 6:3–7. [PubMed: 11789963]
5. Schwartz RS, Henry TD. Pathophysiology of coronary artery restenosis. Rev. Cardiovasc Med. 2002; 3:S4–S9. [PubMed: 12478229]
6. Yahagi K, Otsuka F, Sakakura K, et al. Pathophysiology of superficial femoral artery in-stent restenosis. J. Cardiovasc Surg. 2014; 55:307–323. [PubMed: 24755699]
7. Moreno PR, Fallon JT, Murcia AM, et al. Tissue characteristics of restenosis after percutaneous transluminal coronary angioplasty in diabetic patients. J. Am. Coll. Cardiol. 1999; 34:1045–1049. [PubMed: 10520788]
8. Edlin RS, Tsai S, Yamanouchi D, et al. Characterization of primary and restenotic atherosclerotic plaque from the superficial femoral artery: potential role of Smad3 in regulation of SMC proliferation. J. Vasc. Surg. 2009; 49:1289–1295. [PubMed: 19394554]
9. Inoue S, Koyama H, Miyata T, et al. Pathogenetic heterogeneity of in-stent lesion formation in human peripheral arterial disease. J. Vasc. Surg. 2002; 35:672–678. [PubMed: 11932661]
10. Bauters C, Isner JM. The biology of restenosis. Prog. Cardiovasc Dis. 1997; 40:107–116. [PubMed: 9327827]
11. Longtine JA, Pinkus GS, Fujiwara K, et al. Immunohistochemical localization of smooth muscle myosin in normal human tissues. J. Histochem Cytochem. 1985; 33:179–184. [PubMed: 3882826]
12. Goel SA, Guo LW, Liu B, et al. Mechanisms of post-intervention arterial remodelling. Cardiovas Res. 2012; 96:363–371.
13. Miura A. Apoptotic and nonapoptotic caspase functions in animal development. Cold Spring Harb. Symp. Persp Biol. 2012; 4:1–16.
14. Decker P, Muller S. Modulating poly (ADP-ribose) polymerase activity: potential for the prevention and therapy of pathogenic situations involving DNA damage and oxidative stress. Curr. Pharm. Biotechnol. 2002; 3:275–283. [PubMed: 12164482]
15. Tiggelman AM, Boers W, Linthorst C, et al. Interleukin-6 production by human liver (myo)fibroblasts in culture. Evidence for a regulatory role of LPS, IL-1 beta and TNF alpha. J. Hepatol. 1995; 23:295–306. [PubMed: 8550994]
16. Hendrayani SF, Al-Khalaf HH, Aboussekhra A. The cytokine IL-6 reactivates breast stromal fibroblasts through transcription factor STAT3-dependent upregulation of the RNA-binding protein AUF1. J. Biol. Chem. 2014; 289:30962–30976. [PubMed: 25231991]
17. Habiel DM, Hogaboam C. Heterogeneity in fibroblast proliferation and survival in idiopathic pulmonary fibrosis. Front. Pharmacol. 2014; 5:2. [PubMed: 24478703]
18. Pechkovsky DV, Prele CM, Wong J, et al. STAT3-mediated signaling dysregulates lung fibroblast-myofibroblast activation and differentiation in UIP/IPF. Am. J. Pathol. 2012; 180:1398–1412. [PubMed: 22322297]
19. Shi Y, O'Brien JE Jr, Ala-Kokko L, et al. Origin of extracellular matrix synthesis during coronary repair. circulation. 1997; 95:997–1006. [PubMed: 9054763]
20. Gabbiani G. The myofibroblast in wound healing and fibrocontractive diseases. J Pathol. 2003; 200:500–503. [PubMed: 12845617]
21. Chaudhuri V, Karasek MA. Mechanisms of microvascular wound repair II. Injury induces transformation of endothelial cells into myofibroblasts and the synthesis of matrix proteins. Vitro Cell Dev Biol Anim. 2006; 42:314–319.

22. Kirk TZ, Mark ME, Chua CC, et al. Myofibroblasts from scleroderma skin synthesize elevated levels of collagen and tissue inhibitor of metalloproteinase (TIMP-1) with two forms of TIMP-1. J. Biol. Chem. 1995; 270:3423–3428. [PubMed: 7852429]
23. Schmidt MR, Maeng M, Kristiansen SB, et al. The natural history of collagen and alpha-actin expression after coronary angioplasty. Cardiovasc Pathol. 2004; 13:260–267. [PubMed: 15358340]
24. Lu P, Wang S, Cai W, et al. Role of TGF-beta1/Smad3 signaling pathway in secretion of type I and III collagen by vascular smooth muscle cells of rats undergoing balloon injury. J. Biomed. Biotechnol. 2012:965953. [PubMed: 23091366]
25. Bayes-Genis A, Campbell JH, Carlson PJ, et al. Macrophages, myofibroblasts and neointimal hyperplasia after coronary artery injury and repair. Atherosclerosis. 2002; 163:89–98. [PubMed: 12048125]
26. Wilcox JN, Okamoto EI, Nakahara KI, et al. Perivascular responses after angioplasty which may contribute to postangioplasty restenosis: a role for circulating myofibroblast precursors? Ann. N Y Acad. Sci. 2001; 947:68–90. dicussion 90–2. [PubMed: 11795311]
27. Zalewski A, Shi Y. Vascular myofibroblasts. Lessons from coronary repair and remodeling. Ann. N. Y. Acad. Sci. 1997; 17:417–422.
28. Shi Y, O'Brien JE, Fard A, et al. Adventitial myofibroblasts contribute to neointimal formation in injured porcine coronary arteries. Circulation. 1996; 94:1655–1664. [PubMed: 8840858]
29. Shi Y, O'Brien JE Jr, Fard A, et al. Transforming growth factor-beta 1 expression and myofibroblast formation during arterial repair. Arterioscler. Thromb. Vasc. Biol. 1996; 16:1298–1305. [PubMed: 8857928]
30. Purushothaman KR, Purushothaman M, Muntner P, et al. Inflammation, neovascularization and intra-plaque hemorrhage are associated with increased reparative collagen content: implication for plaque progression in diabetic atherosclerosis. Vasc. Med. 2011; 16:103–108. [PubMed: 21511672]
31. Klair JS, Yang JD, Abdelmalek MF. A longer duration of estrogen deficiency increases fibrosis risk among postmenopausal women with nonalcoholic fatty liver disease. Hepatology. 2016; 64:85–91. [PubMed: 26919573]
32. Krishnan P, Purushothaman KR, Purushothaman M, et al. Relation of internal elastic lamellar layer disruption to neointimal cellular proliferation and type III collagen deposition in human peripheral artery restenosis. Am. J. Cardiol. 2016; 7:1173–1179. [PubMed: 26857165]
33. Bochaton-Piallat ML, Gabbiani G. Modulation of smooth muscle cell proliferation and migration: role of smooth muscle cell heterogeneity. Handb. Exp. Pharmacol. 2005:645–663. [PubMed: 16596818]
34. Mawatari K, Liu B, Kent KC. Activation of integrin receptors is required for growth factor-induced smooth muscle cell dysfunction. J. Vasc. Surg. 2000; 31:375–381. [PubMed: 10664505]
35. Ip JH, Fuster V, Badimon L, et al. Syndromes of accelerated atherosclerosis: role of vascular injury and smooth muscle cell proliferation. J. Am. Col. Cardiol. 1990; 15:1667–1687.
36. Siow RC, Mallawaarachchi CM, Weissberg PL. Migration of adventitial myofibroblasts following vascular balloon injury: insights from in vivo gene transfer to rat carotid arteries. Cardiovasc Res. 2003; 59:212–221. [PubMed: 12829192]
37. Wilcox WR, Waksman R, King SB, et al. The role of the adventitia in the arterial response to angioplasty: the effect of intravascular radiation. Int. J. Radiat. Oncol. Biol. Phys. 1996; 36:789–796. [PubMed: 8960504]
38. Hinz B, Phan SH, Thannickal VJ, et al. The myofibroblast: one function, multiple origins. Am. J. Pathol. 2007; 170:1807–1816. [PubMed: 17525249]
39. Eyden B. The myofibroblast: an assessment of controversial issues and a definition useful in diagnosis and research. Ultrastruct. Pathol. 2001; 25:39–50. [PubMed: 11297318]
40. Moodley YP, Misso NL, Scaffidi AK, et al. Inverse effects of interleukin-6 on apoptosis of fibroblasts from pulmonary fibrosis and normal lungs. Am. J. Respir. Cell Mol. Biol. 2003; 29:490–498. [PubMed: 12714376]
41. Moodley YP, Scaffidi AK, Misso NL, et al. Fibroblasts isolated from normal lungs and those with idiopathic pulmonary fibrosis differ in interleukin-6/gp130-mediated cell signaling and proliferation. Am. J. Pathol. 2003; 163:345–354. [PubMed: 12819039]

42. Akasaka Y, Ono I, Kamiya T, et al. The mechanisms underlying fibroblast apoptosis regulated by growth factors during wound healing. J. Pathol. 2010; 221:285–299. [PubMed: 20527022]
43. Lim MJ, Ahn J, Yi JY, et al. Induction of galectin-1 by TGF-beta1 accelerates fibrosis through enhancing nuclear retention of Smad2. Exp. Cell Res. 2014; 326:125–135. [PubMed: 24928277]
44. Koh DW, Dawson TM, Dawson VL. Mediation of cell death by poly(ADPribose) polymerase-1. Pharmacol. Res. 2005; 52:5–14. [PubMed: 15911329]
45. Zalewski A, Shi Y, Johnson AG. Diverse origin of intimal cells: smooth muscle cells, myofibroblasts, fibroblasts, and beyond? Circ. Res. 2002; 91:652–655. [PubMed: 12386139]
46. Malik N, Francis SE, Holt CM, et al. Apoptosis and cell proliferation after porcine coronary angioplasty. Circulation. 1998; 98:1657–1665. [PubMed: 9778332]
47. Forte A, Della Corte A, De Feo M, et al. Role of myofibroblasts in vascular remodelling: focus on restenosis and aneurysm. Cardiovasc Res. 2010; 88:395–405. [PubMed: 20621923]

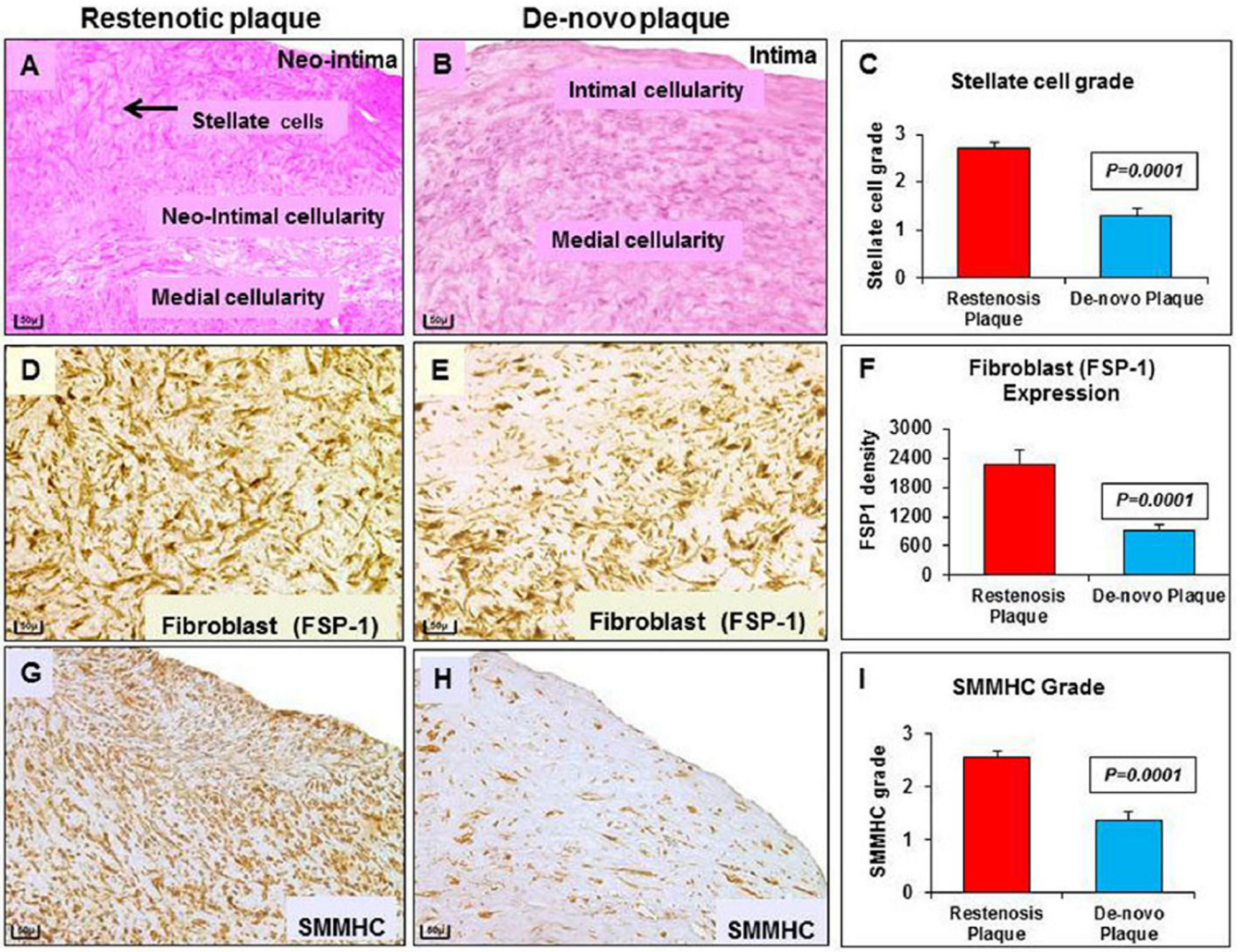

Fig. 1. Stellate cell, fibroblast and SMMHC distribution in restenosis

(A) H&E stain of the restenotic plaque shows "stellate cells" in the neointima, with increased cellularity compared to (B) the intima of *de novo* plaque (20×). (C) Significant difference in stellate cell grade between restenosis and *de novo* plaque. (D) Immunostained section for fibroblasts with FSP-1 shows increased expression in restenotic plaque compared to (E) *de novo* plaques (20×). (F) Significant increase in fibroblast density in restenotic plaques. (G) SMMHC immunostained section in restenotic plaque shows increased protein expression compared to (H) *de novo* plaque. (I) Significant increase in SMMHC in restenotic plaque. Scale bar = 50 μm.

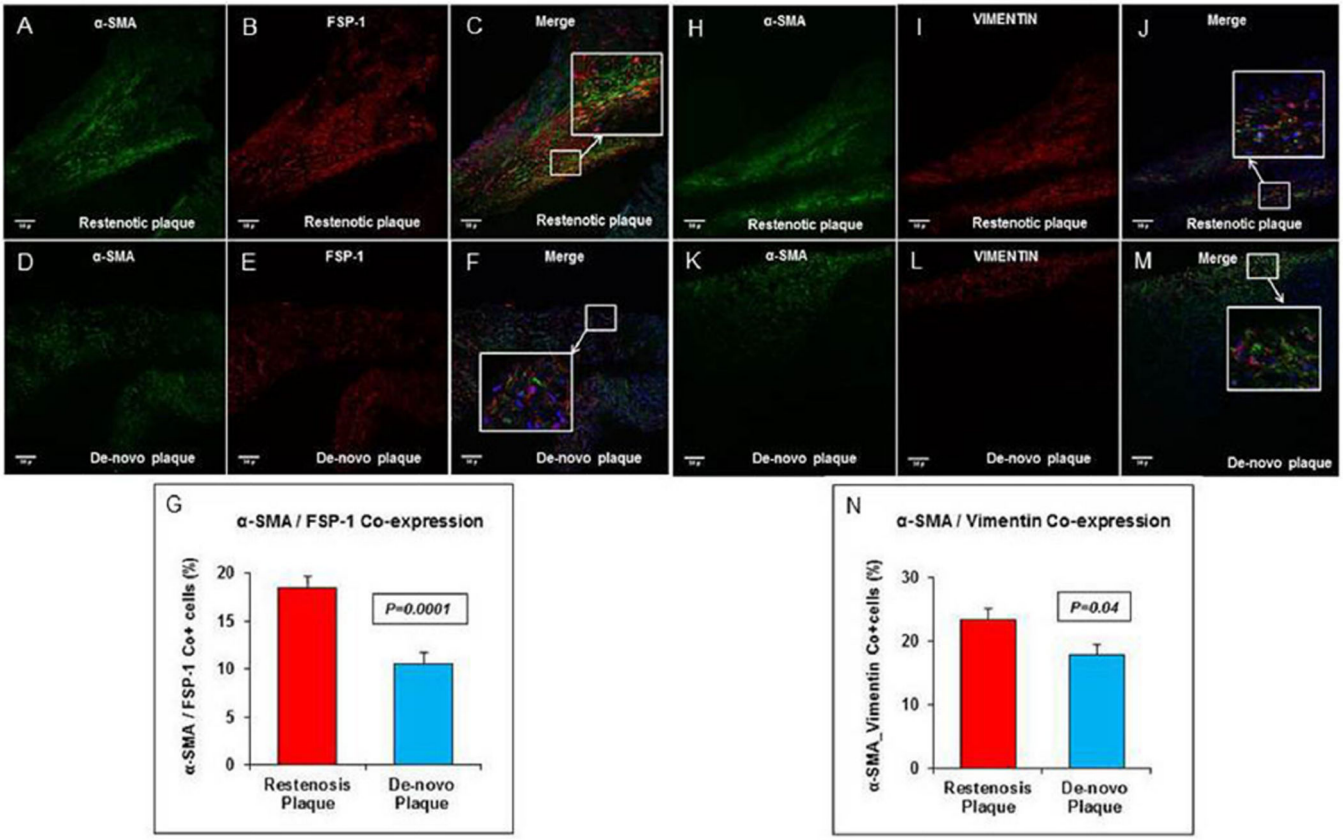

Fig. 2. Myofibroblast α-SMA/FSP-1 co-expression in restenosis

(A) Upper column: immunofluorescence stain shows α-SMA (green) (A) and FSP-1 (red) (B) with merge (C) image at 20×, and the inset shows the magnified view of cells that co-express α-SMA and FSP-1 in restenotic plaques. Increased co-expression of α-SMA with FSP-1 is seen in restenotic compared to *de novo* plaque, lower column (D–F). (G) Comparison between percent of cells that co-express α-SMA and FSP-1 in restenotic plaques *versus de novo* plaque. (B) Upper column: immunofluorescence stain shows α-SMA (green) (H) and vimentin (red) (I) with merge (J) image at 20×, and the inset shows the magnified view in restenotic plaque. Increased co-expression of α-SMA with vimentin is seen in restenotic plaque compared to *de novo* plaque, lower column (K–M). (N) Comparison between percent cells that co-express α-SMA and vimentin in restenotic plaques *versus de novo* plaque. Scale bar = 50 μm. (For interpretation of the references to colour in this figure legend, the reader is referred to the web version of this article.)

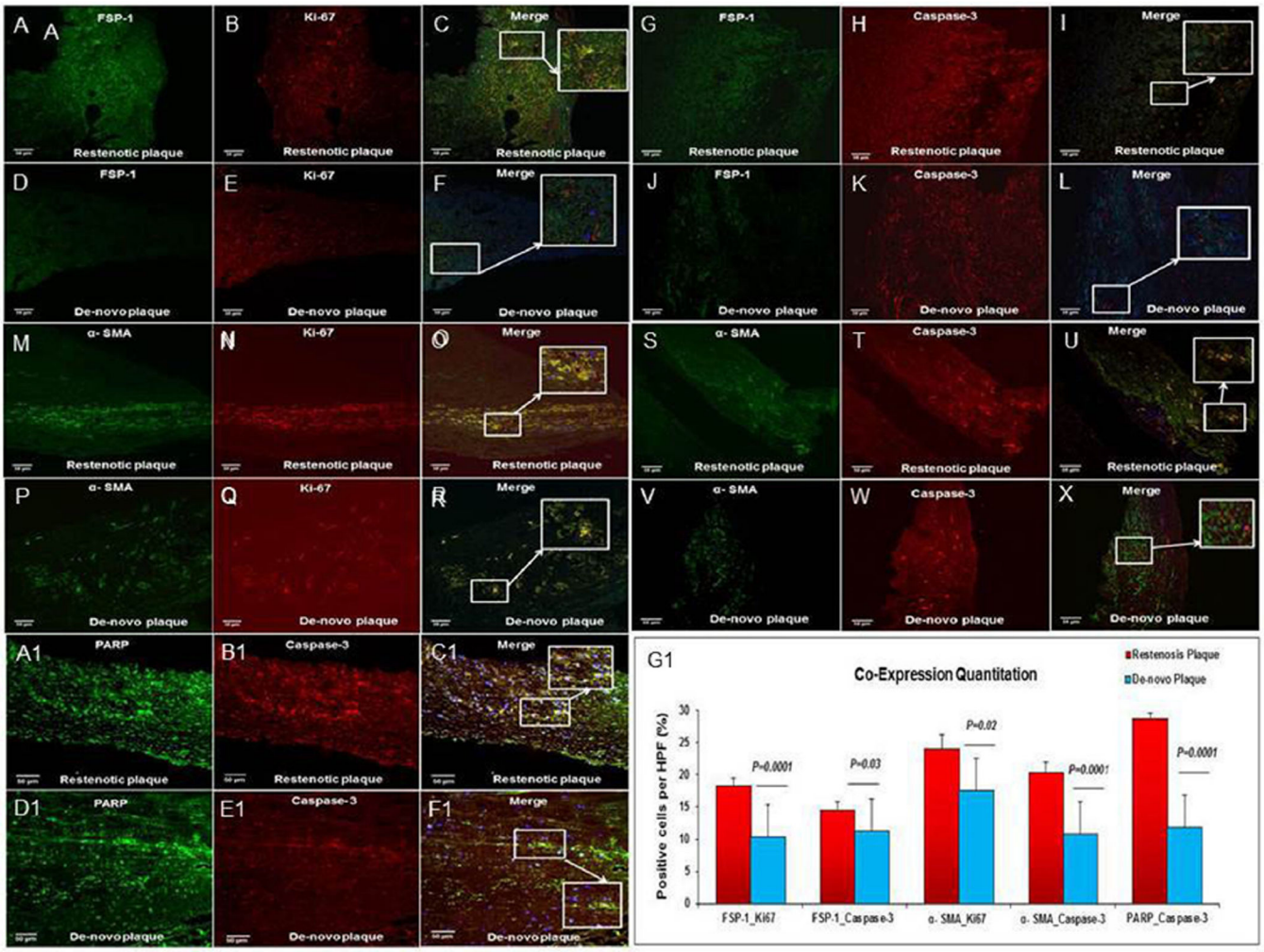

Fig. 3. FSP-1, α-SMA, co-expression with Ki67 and caspase-3 with PARP in restenosis

(A–F) Fibroblast proliferation: immunofluorescence shows FSP-1+ (green) exhibiting Ki-67 (red) expression. The inset is a magnified view. Increased co-expression of FSP-1 and Ki-67 is seen in restenotic plaques compared to *de novo* plaque. (G–L) Fibroblast apoptosis: the immunofluorescence shows FSP-1 (green) exhibiting caspase-3 (red) expression. The inset is a magnified view. Increased co-expression of FSP-1 and caspase-3 is seen in restenotic plaques compared to *de novo* plaque. (M–R) SMC proliferation: immunofluorescence shows SMC, α-SMA positive (green) exhibiting Ki67 (red) expression. The inset is a magnified view. Increased co-expression of α-SMA with Ki67 is seen in restenotic plaques compared to *de novo* plaque. (S–X) SMC apoptosis: immunofluorescence shows SMC, α-SMA (green) exhibiting caspase-3 (red) expression. The inset is a magnified view. Increased co-expression of α-SMA + SMC (green) and active caspase-3 (red) is seen in restenotic plaques compared to *de novo* plaque. Scale bar = 50 μm. (A1–F1) Immunofluorescence revealing PARP+ (green) positive cells exhibiting caspase-3 (red) expression. The inset is a magnified view. Increased co-expression of PARP+ and caspase-3 is seen in restenotic plaques compared to *de novo* plaque. (G1) Significant increase in percentage of co-positive cells per high power field (HPF) in restenotic plaques compared to *de novo* plaques in the

corresponding profiles. (For interpretation of the references to colour in this figure legend, the reader is referred to the web version of this article.)

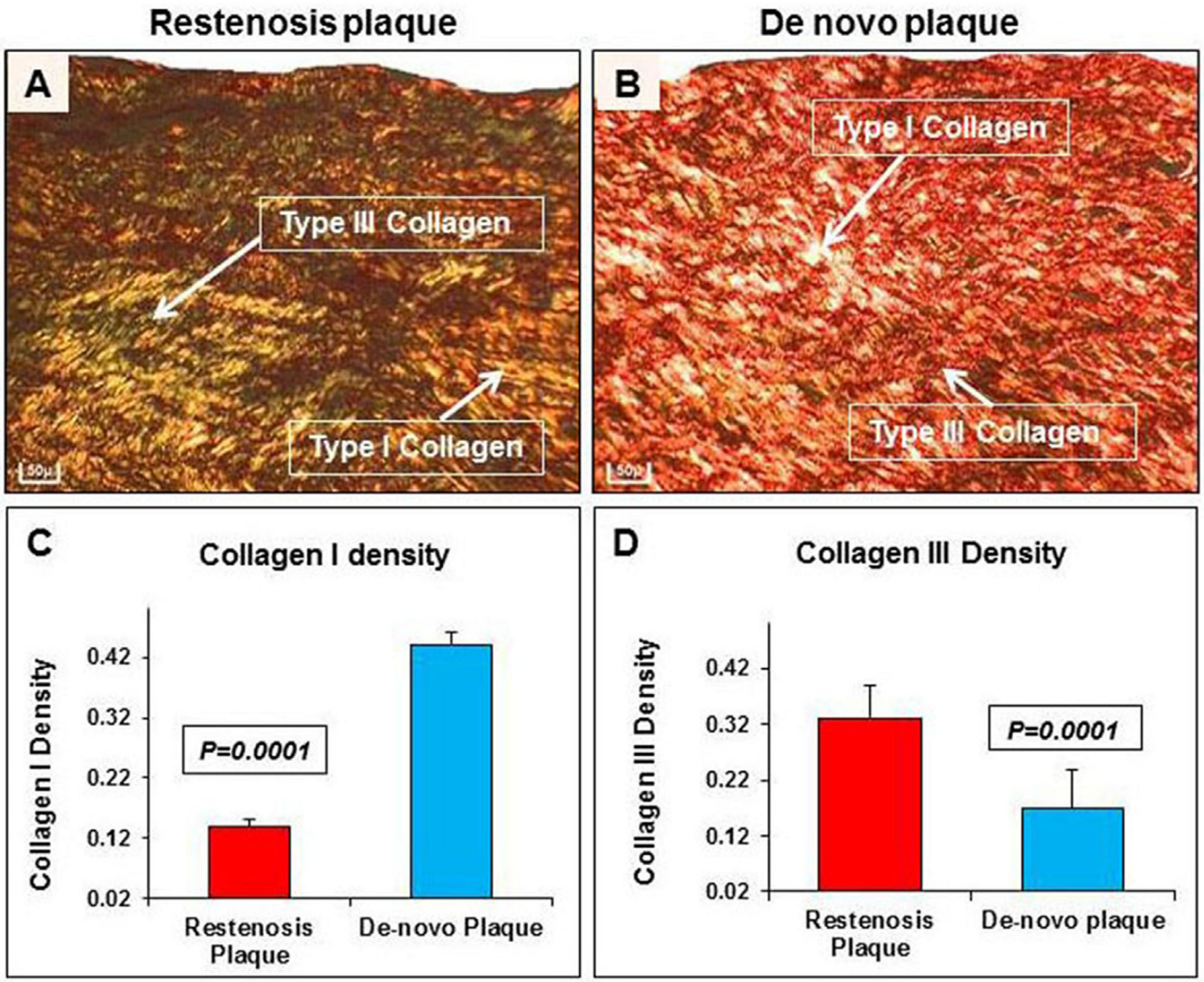

Fig. 4. Collagen distribution in restenosis

(A) Collagens, stained by picro-sirius red stain, show increased type III collagen, indicated by an arrow (green), and reduced type I collagen, indicated by an arrow (red), in restenotic plaques compared to (B) *de novo* plaque (20×). Significant increase in type III collagen in restenotic (C) compared to *de novo* plaque (D). Scale bar = 50 μm. (For interpretation of the references to colour in this figure legend, the reader is referred to the web version of this article.)

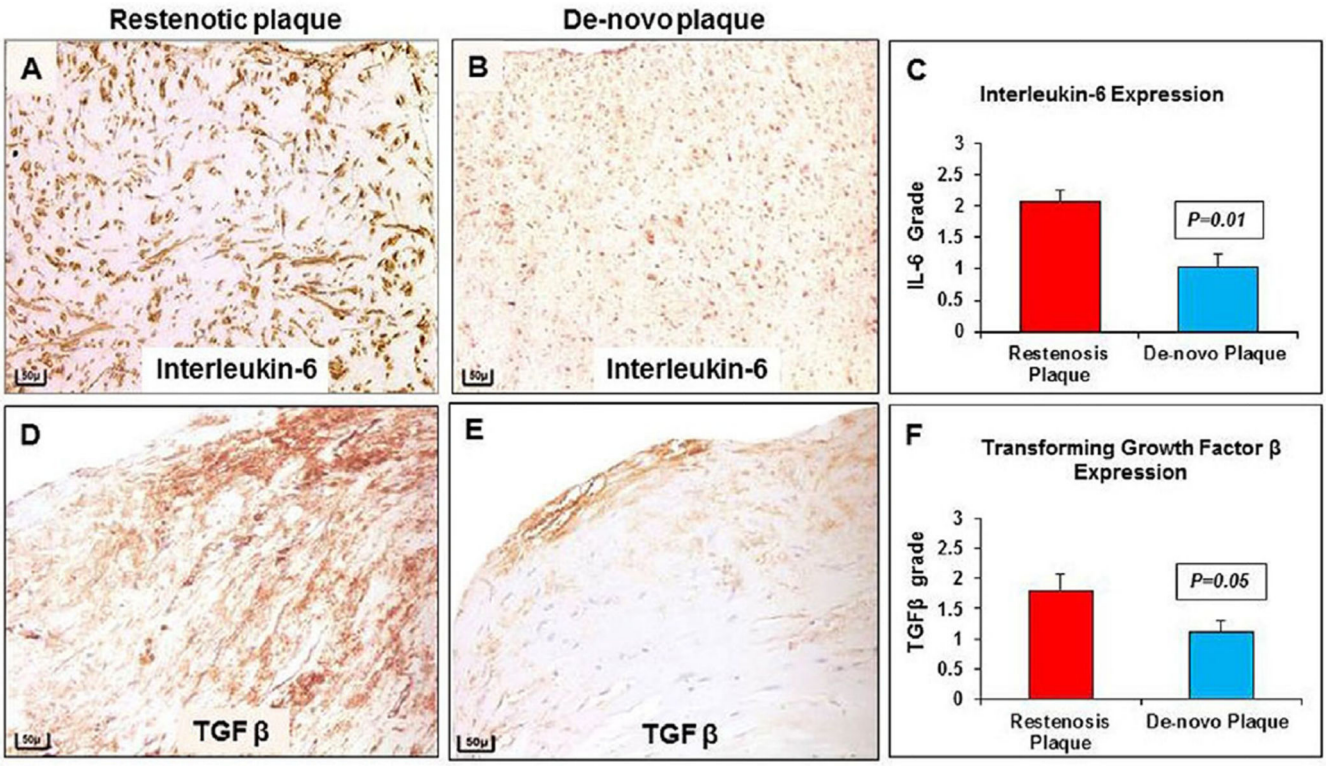

Fig. 5. Interleukin-6 and TGF-β distribution in restenosis

(A) Immunostained section for IL-6 shows increased expression in restenotic plaque compared to (B) *de novo* plaque (20×). (C) Significant increase in IL-6 expression in restenotic compared to *de novo* plaque. (D) Immunostained section for TGF-β shows increased expression in restenotic plaque compared to (E) *de novo* plaque (20×). (F) Significant increase in TGF-β expression in restenotic, compared to *de novo* plaque. Scale bar = 50 μm.

Table 1

Baseline characteristics stratified by presence or absence of restenosis.

Variable	Restenosis (n = 12)	*De novo* control (n = 12)	*p*-value
Age, years	66.1 ± 9.3	65.2 ± 10.0	0.80
Male gender, %	42%	85%	0.02
Body mass index (kg/m^2)	29.3 ± 5.3	25.3 ± 2.6	0.03
Coronary artery disease, %	74%	46%	0.11
Claudication, %	89%	100%	0.23
Rest pain, %	74%	31%	0.02
Smoking, %	68%	85%	0.30
Hypertension, %	100%	100%	N/A
Total cholesterol (mg/dl)	159 ± 53.9	161.7 ± 42.6	0.88
Hemoglobin (gm/dl)	12.3 ± 1.9	13.1 ± 1.4	0.24
Diabetes mellitus, %	63%	46%	0.34
Serum creatinine (mg/dl)	1.1 ± 0.7	1.2 ± 0.4	0.50
Degree stenosis, %	89.5 ± 10.1	82.7 ± 8.8	0.06

Numbers represent mean ± standard deviation or percentage.

n = number of subjects studied.